PERGAMON

Engineering Fracture Mechanics 64 (1999) 87–104

Engineering Fracture Mechanics

www.elsevier.com/locate/engfracmech

A strain gage method for determination of fracture parameters in bimaterial systems

Prabhakar R. Marur, Hareesh V. Tippur*

Department of Mechanical Engineering, Auburn University, Auburn, AL 36849, USA

Received 29 January 1999; accepted 25 March 1999

Abstract

A simple technique for complex stress intensity factor (SIF) determination in a bimaterial crack using electrical strain gages is developed. The asymptotic radial and hoop strain equations are used to compute the SIF by linear transformation. The location of the strain gage relative to the crack tip is chosen through parametric study of the asymptotic fields. The need for higher order terms of the series solution to describe the strain distribution at the gage location is discussed, and a correction procedure using higher order terms is introduced. Static and dynamic experiments are conducted on epoxy/glass-filled epoxy bimaterial specimens in three point bend configuration. Under static loading conditions, the complex SIF estimated from the measured strains is in good agreement with the finite element results obtained by extrapolation of crack flank displacements. The applicability of the present method for dynamic loading conditions is demonstrated by conducting impact tests in a drop-tower system and comparing the measured data with dynamic finite element analysis. The measured dynamic SIF-time history matches favorably with the numerical simulation. © 1999 Elsevier Science Ltd. All rights reserved.

Keywords: Electrical strain gage; Interface crack; Bimaterial; Complex stress intensity factor; Impact loading

1. Introduction

Multiphase material interfaces are found in many advanced aerospace systems, structural composites, thick film coatings, encapsulation for electronic packaging and microelectronic

* Corresponding author. Tel.: +1-334-844-3327.
E-mail address: htippur@eng.auburn.edu (H.V. Tippur)

0013-7944/99/$ - see front matter © 1999 Elsevier Science Ltd. All rights reserved.
PII: S0013-7944(99)00058-2

solder joints. The interface between the two materials is a plane of low strength and the common mode failure mode in such components is the fracture along the interface. The strength of the bond line thus determines the overall mechanical strength of the whole component. Hence, the determination of fracture toughness of bimaterial interface is important in advanced material systems.

In bimaterials, the stress and displacement fields around the crack tip are intrinsically mixed due to the material mismatch across the interface. The mixity of opening and sliding fracture modes plays an important role in characterizing the bimaterial system and strongly influences the fracture toughness of the interface. Experiments have shown that the interface strength of metal/polymer and ceramic/polymer systems is strongly influenced by the mode mixity.

In the experimental determination of stress intensity factor (SIF) in a bimaterial, whole-field optical methods such as laser speckles, coherent gradient sensor [1], and photoelasticity [2,3] have been successfully used. The use of electrical strain gages in bimaterial fracture analysis is rather limited, although strain gage techniques developed by Dally and Sanford [4,5] are well established for homogeneous materials, and have since been extended for orthotropic materials [6]. Only recently have strain gages been put to use in interfacial fracture studies [7]. The advantage of a strain gage technique, apart from its simplicity in application, is in the dynamic loading conditions. The use of strain gages significantly reduces the instrumentation requirements and permits computer based data acquisition. Also, the strain gage technique would be of great advantage in the determination of loading rate dependence of fracture toughness, as a large number of specimens must be tested. Hence, simple and adequately accurate strain gage techniques suitable for static and dynamic complex SIF measurement for the interface crack are needed.

As an engineering alternative, finite element calibration of standard test geometries is also used to determine fracture toughness. The essential aspect of this technique is to obtain calibration plots of load versus complex SIF for test geometries suitable for measuring interface fracture toughness. In the experiments, only the load at the instant of fracture initiation needs to be measured to obtain the critical SIF values. For example, O'Dowd et al. [8] have reported calibration curves for a wide range of material combinations for common fracture test geometries. This calibration or key-curve method would be inapplicable for dynamic fracture studies as the calibration curves are obtained using static loading conditions.

In this paper, a simple strain gage method for complex SIF measurement is developed using the asymptotic field equations of the bimaterial crack. The formulation uses both hoop and radial strain equations to estimate the complex SIF. The radial and hoop strains are measured with a biaxial strain rosette mounted near the crack-tip. The strain gage location with respect to the crack-tip is chosen by careful consideration of the field parameters to maximize the sensitivity of measurement and minimize the error in the data reduction scheme. The need for higher order correction for correlating measured strains to SIF is discussed and a correction scheme is introduced. The present method is applied for measuring complex SIF in a epoxy/glass-filled epoxy bimaterial under quasi-static and dynamic loading conditions.

A brief discussion on the fundamentals of bimaterial crack analysis is presented before the details of formulation, the finite element scheme used for the verification of the test results and the experimental procedure are presented.

2. Interface crack model

Consider an interface crack lying in the bond line between two homogeneous isotropic elastic materials that are otherwise perfectly bonded as shown in Fig. 1. Let μ,E and ν be the shear modulus, Young's modulus and Poisson's ratio of the materials, respectively. The linear elastic solution in the crack tip region is developed using the bimaterial constant ϵ (also known as oscillation index) given by

$$\epsilon = \frac{1}{2\pi}\ln\frac{1-\beta}{1+\beta}, \tag{1}$$

where β is one of the two Dundurs parameters [9].

A Williams' type expansion of the near-tip field using well-known Muskhelishvilli complex potentials is generated as described in [10]. The complete series solutions for the stresses are given in Appendix A. The asymptotic near-tip stress field can be expressed as

$$\sigma_{ij} \sim \frac{1}{\sqrt{r}}\left[K_1\Sigma_{ij}^{\mathrm{I}}(\theta,\ln r;\epsilon) + K_2\Sigma_{ij}^{\mathrm{II}}(\theta,\ln r;\epsilon)\right], \quad i,j = x,y. \tag{2}$$

From the above equation it can be seen that the bimaterial cracks are always intrinsically mixed mode regardless of the nature of the remote loading conditions. Therefore, a complex SIF is defined as $\mathbf{K} = K_1 + iK_2$ such that it reduces to $K_{\mathrm{I}} + iK_{\mathrm{II}}$ if the material mismatch is

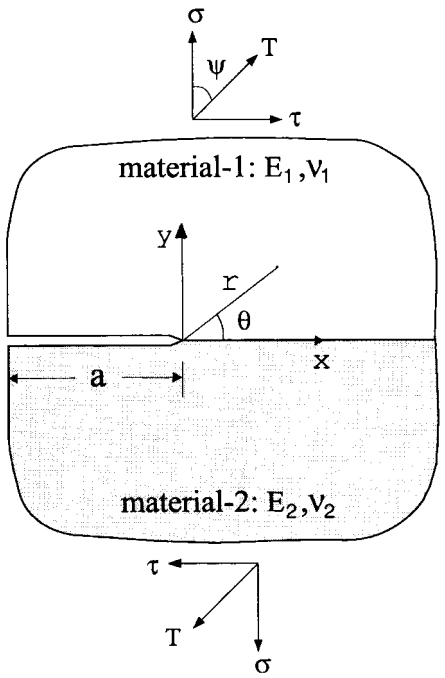

Fig. 1. Interface crack and the coordinate system.

zero, where K_I and K_{II} are SIFs associated with pure mode-I and mode-II loading. The complex SIF is related to the stresses by the following relation

$$\left(\sigma_{yy} + i\sigma_{xy}\right)_{\theta=0} = \frac{\mathbf{K}}{\sqrt{2\pi r}} r^{i\epsilon}, \tag{3}$$

and to the crack-face displacements through

$$(v + iu)_{\theta=\pi} - (v + iu)_{\theta=-\pi} = \frac{c_1 + c_2}{2\sqrt{2\pi}(1 + 2i\epsilon)\cosh(\pi\epsilon)} \mathbf{K}\sqrt{r}(r^{i\epsilon}), \tag{4}$$

in the original form proposed by Hutchinson et al. [11], where $c_i = (\kappa_i + 1)/\mu_i$, $i = 1,2$.

The ratio of the individual SIF components is known as the mode-mixity and it can be computed as the ratio of the shear to normal stresses ahead of the crack tip, or alternatively as the ratio of sliding to opening displacements of the crack flanks. Using an arbitrary length parameter L introduced by Rice [12], the mode mixity ψ is given by

$$\psi = \tan^{-1}\left[\frac{\Im(\mathbf{K}L^{i\epsilon})}{\Re(\mathbf{K}L^{i\epsilon})}\right]. \tag{5}$$

Following Sun and Jih [13], the value of L is set to $2a$, where a is the crack length.

Due to the oscillatory singularity, the linear elastic solution predicts inter-penetration of crack faces even for internal pressure loading of the crack faces, and the presence of this contact zone clouds the definitions of fracture parameters for the bimaterial crack. Rice [12] has advanced a small-scale contact model wherein the contact zone can be ignored, provided certain conditions on the remote loading is met. Defining the remote loading mixity Ψ as

$$\Psi = \tan^{-1}\left(\frac{\sigma_{xy}^{\infty}}{\sigma_{yy}^{\infty}}\right), \tag{6}$$

and taking $\epsilon = 0.15$, which could be considered as the largest feasible value for combination of two homogeneous solids with positive Poisson's ratios, Rice [12] has shown that the contact zone can be neglected as long as $\Psi > -50^{\circ}$. This restriction could easily be met in any practical experimental set-up. For smaller values of mismatch, the restriction on the loading mixity is further relaxed. Hence, under tensile dominated crack loading, such as the ones considered in this paper, the small-scale model would suffice.

3. Numerical determination of SIF

A displacement extrapolation technique is developed using the definition of complex crack opening displacement (COD) to compute the complex SIF in bimaterial specimens. The complex COD, $\boldsymbol{\delta}$ can be defined as a vectorial sum as

$$\boldsymbol{\delta} = \Delta v + i\Delta u, \tag{7}$$

where Δv and Δu are the opening and the sliding displacement jumps across the crack faces.

Considering only the K-dominant terms in the series solution for the bimaterial crack, the relative displacements of the crack faces can be given as

$$\Delta u(r) = u(r,\pi) - u(r,-\pi) = \gamma\left[F_1(\phi)K_1 + F_2(\phi)K_2\right]\sqrt{2\pi r},$$

$$\Delta v(r) = v(r,\pi) - v(r,-\pi) = \gamma\left[F_2(\phi)K_1 - F_1(\phi)K_2\right]\sqrt{2\pi r}, \tag{8}$$

where

$$F_1(\phi) = \sin(\phi) - 2\epsilon\cos(\phi),$$

$$F_2(\phi) = \cos(\phi) + 2\epsilon\sin(\phi),$$

$$\phi = \epsilon\log\left(\frac{r}{2a}\right),$$

$$\gamma = \frac{c_1 + c_2}{2\sqrt{\pi}(1+2i\epsilon)\cosh(\pi\epsilon)}.$$

The complex COD can be related to the magnitude of the complex SIF factor by

$$|\boldsymbol{\delta}| = \frac{c_1 + c_2}{4\pi\sqrt{1+4\epsilon^2}\cosh(\pi\epsilon)}|\mathbf{K}|\sqrt{2\pi r}. \tag{9}$$

In this formulation, the small region of penetration in the crack face displacements predicted by the linear elasticity is ignored based on Rice's small scale model as the displacements of the nodes lying in r/a of 0.01–0.1 are used to compute SIF. From regression analysis of the nodal displacement data using Eq. (9), the magnitude of $\mathbf{K}$ is obtained.

The mode mixity can be computed from the ratio of sliding and opening displacements using Eq. (8). Representing K_1 and K_2 in terms of Δu and Δv as

$$\begin{Bmatrix} K_1 \\ K_2 \end{Bmatrix} = \frac{1}{\gamma\sqrt{2\pi r}\left[F_1^2(\phi) + F_2^2(\phi)\right]}\begin{bmatrix} F_1(\phi) & F_2(\phi) \\ F_2(\phi) & -F_1(\phi) \end{bmatrix}\begin{Bmatrix} \Delta u \\ \Delta v \end{Bmatrix}, \tag{10}$$

and the ratio of SIFs can be obtained as

$$\frac{K_2}{K_1} = \frac{\left[F_2(\phi)/F_1(\phi)\right](\Delta u/\Delta v) - 1}{(\Delta u/\Delta v) + \left[F_2(\phi)/F_1(\phi)\right]}. \tag{11}$$

The mode mixity is computed by taking the inverse tangent of the ratio of K_2 and K_1.

The numerical implementation of above equation needs further attention. Due to the oscillatory nature of the singular field, it has been suggested that mode mixity be defined as the ratio of shear stress to opening stress at a specific distance from the crack tip [14]. Usually this distance is defined as some characteristic length pertinent to the material under investigation. However, considering that the nodes used in the computation are outside the oscillatory

region, an extrapolation technique can be used to fit a linear equation to the data points, and taking the mode-mixity in the limit r tending to zero as

$$\tan\psi = \lim_{r\to 0}\left(\frac{K_2}{K_1}\right). \tag{12}$$

To demonstrate the accuracy of the displacement approach, a bench mark problem is solved. The problem considered is an edge-crack lying in the bond line between two dissimilar plates

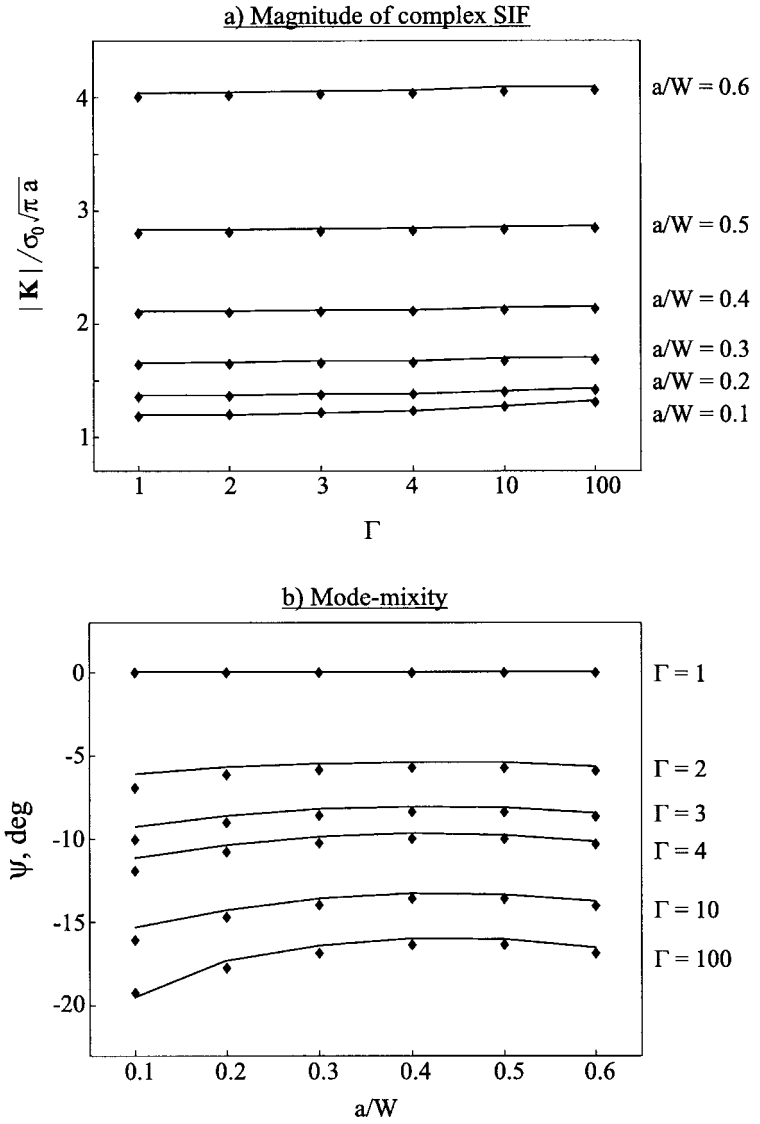

Fig. 2. Comparison of $|\mathbf{K}|$ and ψ computed by COD extrapolation with published results ($\Gamma = E_2/E_1$). ◇◇ present, — [15].

subjected to remote tensile stress σ_0. The Poisson's ratio is 0.3 for both the materials. The analysis is performed for various ratios of Young's moduli denoted by Γ $(= E_2/E_1)$ and the crack length-to-width ratio a/W. The non-dimensional SIF $(= |\mathbf{K}|/\sigma_0\sqrt{\pi a})$ and the mode-mixity are compared with the results reported by Miyazaki et al. [15] in Fig. 2. The $|\mathbf{K}|$ and mode-mixity values agree quite well with published results.

4. Theoretical analysis

The formulation to relate the strain to complex SIF takes in the K-dominant part of the series solution, which has two unknowns namely K_1 and K_2. Hence, a minimum of two strain measurements are required to solve for the SIFs. Ricci et al. [7] have measured radial strains at two different locations, and solved for the SIF values. However, as the strain gage technique must be extendible to dynamic fracture testing, the gages must have the same location to avoid the temporal shift in the strains measured by the two gages. A biaxial rosette mounted at some location r would measure both the radial and hoop strains, providing the required number of data for the formulation. Hence, radial and hoop strain equations are used to evaluate the complex SIF by linear transformation.

The asymptotic equations for the stress field around the bimaterial crack tip can be written as

$$\sigma_{rr} = \frac{1}{\sqrt{r}}\left[K_1\Sigma^{\mathrm{I}}_{rr}(\theta) + K_2\Sigma^{\mathrm{II}}_{rr}(\theta)\right], \tag{13}$$

$$\sigma_{\theta\theta} = \frac{1}{\sqrt{r}}\left[K_1\Sigma^{\mathrm{I}}_{\theta\theta}(\theta) + K_2\Sigma^{\mathrm{II}}_{\theta\theta}(\theta)\right], \tag{14}$$

where

$$\Sigma^{\mathrm{I}}_{rr}(\theta) = \omega\left[2\cos(\theta/2+\phi) + \cos\hat{\theta}_1 + \sin\theta\sin\hat{\theta}_2 + 2\epsilon\cos\hat{\theta}_2\sin\theta\right] - \frac{\cos\hat{\theta}_3}{\omega},$$

$$\Sigma^{\mathrm{II}}_{rr}(\theta) = \omega\left[-2\sin(\theta/2+\phi) + \sin\hat{\theta}_1 - \sin\theta\cos\hat{\theta}_2 + 2\epsilon\sin\hat{\theta}_2\sin\theta\right] + \frac{\sin\hat{\theta}_3}{\omega},$$

$$\Sigma^{\mathrm{I}}_{\theta\theta}(\theta) = \omega\left[2\cos(\theta/2+\phi) - \cos\hat{\theta}_1 - \sin\theta\sin\hat{\theta}_2 - 2\epsilon\cos\hat{\theta}_2\sin\theta\right] + \frac{\cos\hat{\theta}_3}{\omega},$$

$$\Sigma^{\mathrm{II}}_{\theta\theta}(\theta) = \omega\left[-2\sin(\theta/2+\phi) - \sin\hat{\theta}_1 + \sin\theta\cos\hat{\theta}_2 - 2\epsilon\sin\hat{\theta}_2\sin\theta\right] - \frac{\sin\hat{\theta}_3}{\omega},$$

$$\hat{\theta}_1 = 3\theta/2 - \phi,$$

$$\hat{\theta}_2 = \theta/2 - \phi,$$

$$\hat{\theta}_3 = 3\theta/2 + \phi,$$

$$\omega = \exp(-\epsilon(\pi - \theta)),$$

$$\phi = \epsilon \log(r/2a).$$

With a plane stress assumption, the radial and hoop strain equations can be given as

$$\epsilon_{rr} = \frac{1}{E\sqrt{r}}\left[K_1\left(\Sigma^{\mathrm{I}}_{rr} - \nu\Sigma^{\mathrm{I}}_{\theta\theta}\right) + K_2\left(\Sigma^{\mathrm{II}}_{rr} - \nu\Sigma^{\mathrm{II}}_{\theta\theta}\right)\right], \tag{15}$$

$$\epsilon_{\theta\theta} = \frac{1}{E\sqrt{r}}\left[K_1\left(\Sigma^{\mathrm{I}}_{\theta\theta} - \nu\Sigma^{\mathrm{I}}_{rr}\right) + K_2\left(\Sigma^{\mathrm{II}}_{\theta\theta} - \nu\Sigma^{\mathrm{II}}_{rr}\right)\right]. \tag{16}$$

In the above equations, only the compliant half plane of the bimaterial system is considered as that would be the natural choice for strain gage fixing. Hence, the Young's modulus and Poisson's ratio are given in a generic fashion without the subscripts. The above equations can be cast in a matrix form in terms of K_1 and K_2 as

$$\begin{Bmatrix} K_1 \\ K_2 \end{Bmatrix} = E\sqrt{r}\begin{bmatrix} \left(\Sigma^{\mathrm{I}}_{rr} - \nu\Sigma^{\mathrm{I}}_{\theta\theta}\right) & \left(\Sigma^{\mathrm{II}}_{rr} - \nu\Sigma^{\mathrm{II}}_{\theta\theta}\right) \\ \left(\Sigma^{\mathrm{I}}_{\theta\theta} - \nu\Sigma^{\mathrm{I}}_{rr}\right) & \left(\Sigma^{\mathrm{II}}_{\theta\theta} - \nu\Sigma^{\mathrm{II}}_{rr}\right) \end{bmatrix}^{-1} \begin{Bmatrix} \epsilon_{rr} \\ \epsilon_{\theta\theta} \end{Bmatrix}, \tag{17}$$

from which the complex SIF can be estimated once the radial and hoop strains are available.

The choice of r and θ for mounting the strain rosette should be such that the conditioning of the coefficient matrix is minimized, and the sensitivity of the strain measurements is maximized.

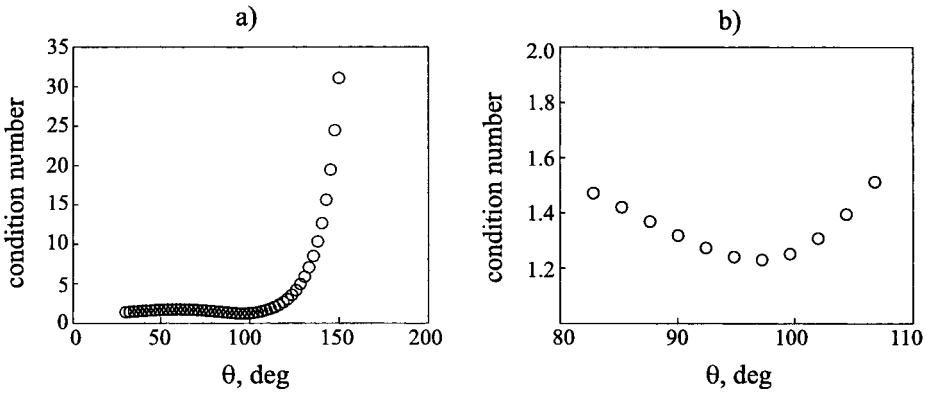

Fig. 3. (a) Matrix condition number with respect to matrix inversion. ($\epsilon = 0.05$). (b) Expanded view for θ from 80° to 110°.

Also the gages must be located in the region prescribed by $r \geq 0.5B$, where B is the thickness of the specimen and $30^\circ \geq \theta \leq 150^\circ$, for plane stress conditions to prevail [16,17]. Usually, the radial distance r is in the range from $0.5B$ to $0.6B$. Larger radii would result in significant reduction in the strain and would also place the gage outside the K-dominant region. At smaller radii, strain-averaging effect of the electrical strain gage must be considered due to the sharp strain gradients around the crack-tip. Ricci [7] have shown by parametric study that the sensitivity curves flatten beyond $r/B = 0.4$, and the strain-averaging error is less than 0.2% if r/B is greater than 0.4. Hence, in this paper, the gage is mounted at a radial distance of $0.6B$ which ensures that the active grid of the strain gage is outside the 3D zone.

The mounting angle θ must be chosen to ensure that the coefficient matrix in Eq. (17) is well conditioned to reduce errors in the matrix inversion. Fig. 3 shows the matrix condition number of the coefficient matrix for a mismatch parameter of 0.05. It can be observed from the figure that the system becomes ill-conditioned for θ approaching 150° and least conditioning number is achieved for an angle of 97.5°. The angles for best conditioning for different mismatch parameters are shown in Fig. 4. The optimum angle for strain gage mounting falls in the range from 85 to 100° for most common values of ϵ and ν.

Within the narrow range of angles necessitated by the matrix conditioning number, a generic mounting angle must be chosen to maximize the sensitivity of the measurement. This angle is determined from the angular distribution of ϵ_{rr} and $\epsilon_{\theta\theta}$ at a specific radius for different mismatch parameters. Fig. 5 shows the angular variation of radial and hoop strain for different mismatch parameters at $r/B = 0.6$. The peak radial and hoop strains occur in the neighborhood of $\theta = 90^\circ$ for the entire range of material mismatch parameters considered. Hence, a value of 90° could be used as a common angle for most bimaterial combinations. The mounting angle of 90° considerably simplifies the strain gage fixing, as no extra angle marking and alignment are necessary. Hence, the optimal location for the strain rosette would be $r = 0.6B$ and $\theta = 90^\circ$ on the compliant side of the bimaterial.

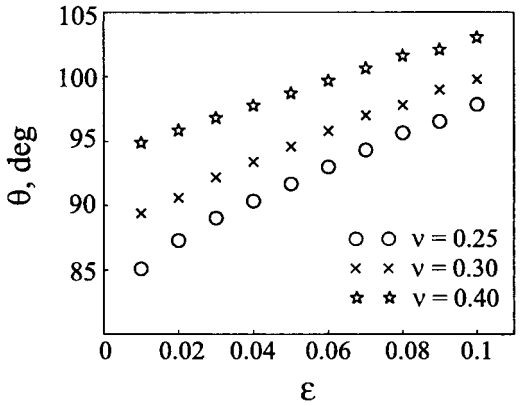

Fig. 4. Strain gage mounting angles for different mismatch parameters.

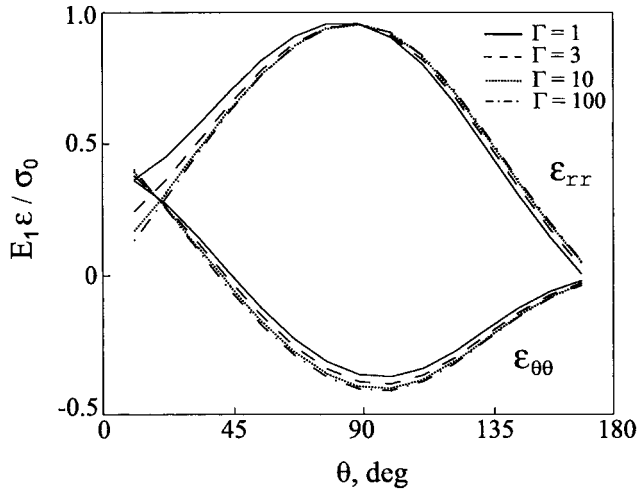

Fig. 5. Radial and hoop strains at $r = 0.6B$ for different material combinations ($\Gamma = E_2/E_1$).

5. Experimental Procedure

Static experiments are conducted on epoxy based bimaterial specimens to measure SIF using the strain gage technique developed here. Bimaterial samples are fabricated by joining pure epoxy and glass-filled epoxy specimen halves with epoxy resin. Uncoated solid glass spheres with mean diameter of 33 μm are used as fillers in epoxy. The bonding surfaces are roughened with 240-grit emery, and the surfaces are subsequently cleaned with laboratory-grade isopropyl alcohol. The specimen halves are then positioned in an acrylic mould and a thin layer of epoxy resin is applied over the bonding surfaces. Light clamping pressure is applied from the free ends, and the sample is allowed to cure for seven days.

The static material properties are measured using strain gages, and the dynamic properties are evaluated using ultrasonic wave velocity measurements as described in Ref. [18]. The static and dynamic properties are listed in Table 1. The samples are machined to the final dimensions shown in Fig. 6. Three specimens are tested under a mid-span load of 100 N in three point bend configuration. A biaxial rosette (CEA-13-032WT-120 from Measurements Group) with gage length of 0.81 mm is mounted at $r = 0.6B$ and $\theta = 90^\circ$ from the crack tip.

Application of the relations developed using the asymptotic solution to the experimental

Table 1
Static and dynamic material properties

Specimen	Static		Dynamic		ρ (kg/m^3)
	E (GPa)	ν	E (GPa)	ν	
Epoxy	3.5	0.35	4.6	0.37	1150
Glass-fill epoxy	10.8	0.29	13.0	0.32	1720

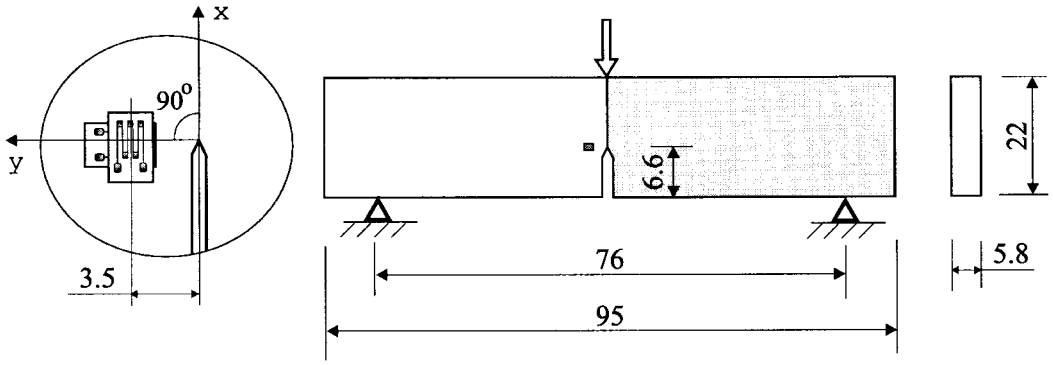

Fig. 6. Specimen geometry and strain gage location. All dimensions in mm.

data yielded a magnitude of complex SIF that agreed reasonably with the finite element value of $|\mathbf{K}| = 0.6$ MPa $m^{1/2}$ and a mode-mixity value that is about three times higher than the numerical value of $\psi = -6.6^\circ$. The estimated SIF values for the three specimens are listed in Table 2. The disagreement in mode-mixity is attributable to the inadequacy of the K-dominant solution to describe the far-field strain distribution. The K-dominant solution for $r = 0.6B$ is compared with finite element results in Fig. 7(a), which clearly shows the inadequacy of the asymptotic solution. Hence, higher order terms are added until satisfactory match is obtained. Fig. 7(b) shows the comparison of FEA results with the analytical solution obtained using first eight-terms in the series.

It is clear from the results plotted in Fig. 7 that higher order terms must be included in the formulation to get adequate accuracy. The Eqs. (15) and (16) can be modified to take the higher order terms into account as

$$E\epsilon_{rr} = r^{-1/2}\left[K_1\left(\Sigma^{\mathrm{I}}_{rr} - \nu\Sigma^{\mathrm{I}}_{\theta\theta}\right) + K_2\left(\Sigma^{\mathrm{II}}_{rr} - \nu\Sigma^{\mathrm{II}}_{\theta\theta}\right)\right] + O(r), \tag{18}$$

$$E\epsilon_{\theta\theta} = r^{-1/2}\left[K_1\left(\Sigma^{\mathrm{I}}_{\theta\theta} - \nu\Sigma^{\mathrm{I}}_{rr}\right) + K_2\left(\Sigma^{\mathrm{II}}_{\theta\theta} - \nu\Sigma^{\mathrm{II}}_{rr}\right)\right] + O(r), \tag{19}$$

where $O(r)$ indicates all the higher order terms in r. To include the higher order terms, the

Table 2
SIF determination for the bimaterial system

Specimen Number	K-dominant solution				higher order solution			
	ϵ_{rr} (με)	$\epsilon_{\theta\theta}$ (με)	$\lvert\mathbf{K}\rvert$ (MPa $m^{1/2}$)	ψ (°)	$\tilde{\epsilon}_{rr}$ (με)	$\tilde{\epsilon}_{\theta\theta}$ (με)	$\lvert\mathbf{K}\rvert$ (MPa $m^{1/2}$)	ψ (°)
Bim-02	1153	−526	0.62	−22.6	1166	−206	0.62	−6.1
Bim-03	1175	−539	0.63	−22.7	1188	−219	0.63	−6.5
Bim-04	1150	−524	0.62	−22.6	1163	−203	0.62	−6.0

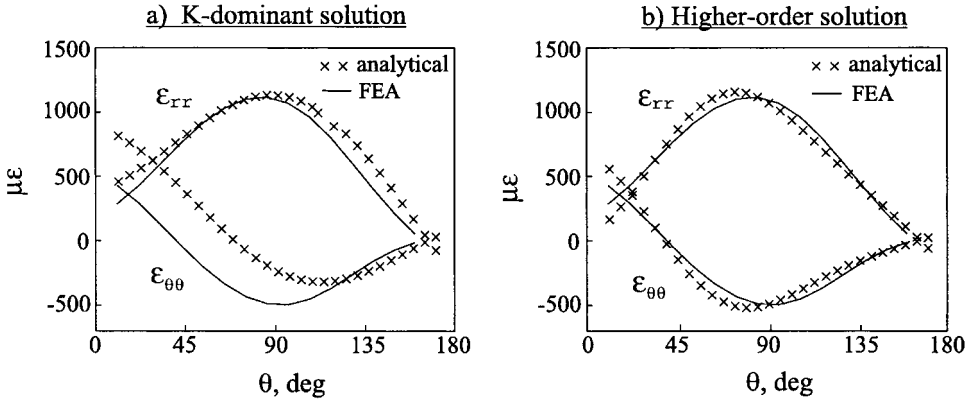

Fig. 7. Comparison of *K*-dominant and higher order solutions with FEA.

coefficients $\mathbf{a}_n$ and $\mathbf{b}_n$ of the series solution given in Appendix A must be evaluated. If the coefficients are left undetermined in the formulation, then at the least, as many strain gages as the number of terms desired are required. For instance, to obtain a eight-term solution, eight strain gages must be used to obtain the SIF data, which would render the strain gage technique impractical. However, a simpler, problem-specific solution is to obtain the coefficients of the boundary value problem once, and compute the correction factors to compensate for the truncation of series in the formulation. The coefficients can be evaluated from optical measurements [19] or can be computed using numerical methods. In this work, the coefficients are evaluated from the FEA results using the least-squares analysis described in Appendix B. The higher order correction needs to be computed only once for a given test specimen configuration, and in addition, it can used be directly for dynamic loading conditions with certain restrictions on the loading rate.

Addition of higher order terms beyond the first eight terms did not result in any appreciable improvement in the agreement with the finite element results. Hence, only the first eight terms are considered in the analysis. Initially, the coefficients for the series solution are computed from the finite element stress data. Using the first two terms of the series, the radial and hoop strains at r and θ corresponding to the strain-gage location are obtained. Then, the strains at the same location are computed using the first eight terms of the series. The difference between the two-term solution and the higher order solution provides the correction factor.

The higher order correction can be applied to the measured strain to obtain the corrected strain $\tilde{\epsilon}_{ij}$ from which SIF can be computed as

$$\begin{Bmatrix} K_1 \\ K_2 \end{Bmatrix} = E\sqrt{r}\begin{bmatrix} \left(\Sigma^{\mathrm{I}}_{rr} - \nu\Sigma^{\mathrm{I}}_{\theta\theta}\right) & \left(\Sigma^{\mathrm{II}}_{rr} - \nu\Sigma^{\mathrm{II}}_{\theta\theta}\right) \\ \left(\Sigma^{\mathrm{I}}_{\theta\theta} - \nu\Sigma^{\mathrm{I}}_{rr}\right) & \left(\Sigma^{\mathrm{II}}_{\theta\theta} - \nu\Sigma^{\mathrm{II}}_{rr}\right) \end{bmatrix}^{-1} \begin{Bmatrix} \tilde{\epsilon}_{rr} \\ \tilde{\epsilon}_{\theta\theta} \end{Bmatrix}. \tag{20}$$

This higher order technique is used to correlate the strains to SIF and the results are listed in Table 2. The finite element values are $|\mathbf{K}| = 0.6\ \mathrm{MPa\,m^{1/2}}$ and $\psi = -6.6^\circ$. The SIF computed from the corrected strain values match reasonably well with the numerical results.

6. Application to dynamic testing

The applicability of the present formulation to impact testing is investigated in this section. The dynamic fracture experiments are conducted on bimaterial samples with the gages mounted at the same location as in the static case. The specimen is impacted with the initial impact velocity of 0.5 m/s. The pertinent strain equations and correction factors derived in the previous section are based on the static strain field around the crack-tip. The same field equations are used in the dynamic loading conditions, as the initial impact velocity is low. The SIF-time history obtained from dynamic fracture experiments are compared with the dynamic finite element simulations.

The impact experiments are conducted using an instrumented drop-tower system. The tup and the support anvil are instrumented to measure the dynamic loads. The load signals and the output from the strain-rosette fixed on the specimen are amplified using high frequency strain amplifiers. The amplified signals are digitized using a 1-MHz data acquisition system. The measured time-histories are shown in Fig. 8.

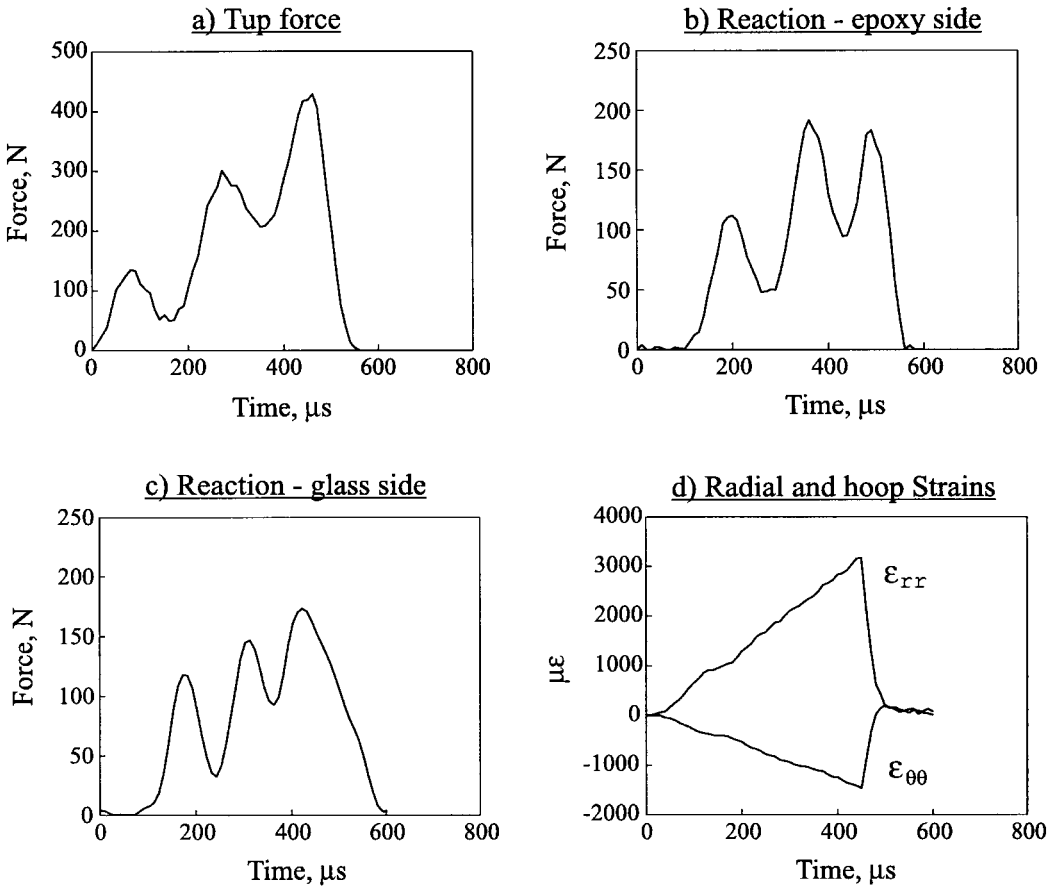

Fig. 8. Impact test data for a bimaterial specimen.

The measured tup force and anvil reaction time histories are applied as traction boundary conditions to a 2D finite element model with eight-noded isoparameteric plane stress elements. The full length of the specimen (including the overhangs) is modeled without imposing any displacement constraints [20]. The dynamic values of the Young's modulus and Poisson's ratio are used in the model.

For the purpose of comparing the measured strain directly with numerical simulations, the radial and hoop strains from a node placed 3.5 mm from the crack-tip (corresponding to the strain gage location) in the finite element model are extracted. The computed strains are compared with the measured data in Fig. 9(a). The agreement between the two is good until the time of fracture ($=428$ μs). Since the measured and computed strain histories match, the SIF-history derived from strain gage measurement would match with the finite element simulation, provided the technique developed here holds good in the dynamic case. The measured strains are transformed to complex SIF-time history using Eq. (20) and they are compared with the SIF-time history computed by finite element analysis in Fig. 9(b). The close agreement between the measured and computed SIF establishes the applicability of the present method in the low-velocity impact tests.

7. Conclusions

A simple technique for complex SIF determination in bimaterials using electrical strain gages is presented. The strain field around the bimaterial crack tip is investigated and pertinent equations to relate the measured strain to SIF using only K-dominant terms is presented. The strain gage location with respect to the crack tip is chosen to minimize the conditioning of the coefficient matrix and to maximize the sensitivity of the measurements. The need for higher order terms to describe the strain field, and the inapplicability of method of undetermined coefficients is discussed. A correction procedure using the higher order terms of the series solution is introduced. The coefficients of the higher order terms are obtained using finite element results in conjunction with least-squares analysis. Static loading experiments are

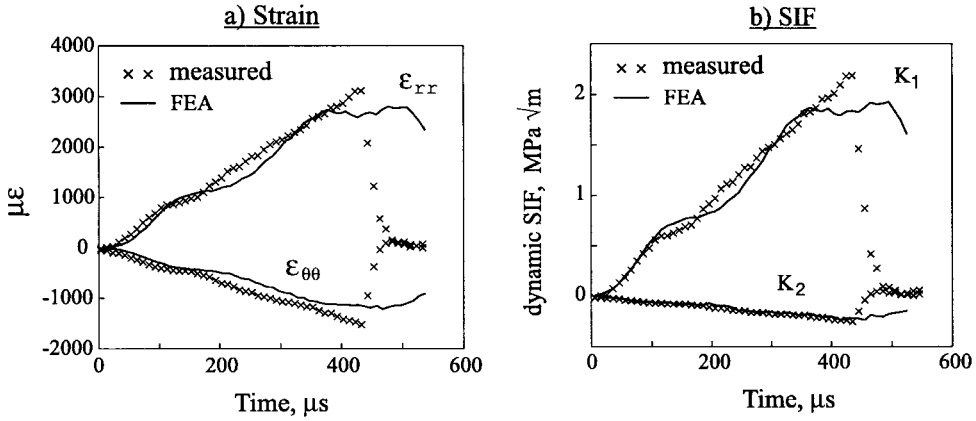

Fig. 9. Comparison of measured strain and SIF with FEA results.

conducted on epoxy/glass-filled epoxy bimaterial system, and the measured SIFs agree quite well with the finite element results obtained using extrapolation of CODs. The applicability of the present method for impact testing is established by using the method to measure complex SIF under low-velocity impact loading. The complex SIF histories obtained from the strain records compare well with finite element simulations until the time of fracture.

Acknowledgements

Support of the research by grants NSF-CMS-9622055 and AF-F49620 is greatfully acknowledged.

Appendix A. Series solution for stresses around a bimaterial crack

The complete series solution for stress field around a crack lying along the bondline between two dissimilar isotropic homogeneous materials is given below.

$$\begin{aligned}\sigma_{rr} = \sum_{n=0}^{N} \Re\left[\bar{\mathbf{a}}_n L^{i\epsilon}\right] r^{n-1/2} \Big\{ \omega \big[2\cos\hat{\theta}_1 + \cos\theta_1 + (1-2n)\sin\hat{\theta}_2 \sin\theta + 2\epsilon\cos\hat{\theta}_2 \sin\theta \big] - \\ \cos\hat{\theta}_3/\omega \Big\} + \Im\left[\bar{\mathbf{a}}_n L^{i\epsilon}\right] r^{n-1/2} \Big\{ \omega \big[2\sin\hat{\theta}_1 + \sin\theta_1 - (1-2n)\cos\hat{\theta}_2 \sin\theta + 2\epsilon\sin\hat{\theta}_2 \\ \sin\theta \big] + \sin\hat{\theta}_3/\omega \Big\} + 4\hat{c}_2 \Re[\mathbf{b}_n] r^n \big[\cos n\theta + \cos(n+2)\theta - n\sin\theta \sin(n+1)\theta \big] + 4\hat{c}_2 \\ \Im[\mathbf{b}_n] r^n \big[-\sin n\theta - n\sin\theta\cos(n+1)\theta \big],\end{aligned} \tag{A1}$$

$$\begin{aligned}\sigma_{\theta\theta} = \sum_{n=0}^{N} \Re\left[\bar{\mathbf{a}}_n L^{i\epsilon}\right] r^{n-1/2} \Big\{ \omega \big[2\cos\hat{\theta}_1 - \cos\theta_1 - (1-2n)\sin\hat{\theta}_2 \sin\theta - 2\epsilon\cos\hat{\theta}_2 \sin\theta \big] + \\ \cos\hat{\theta}_3/\omega \Big\} + \Im\left[\bar{\mathbf{a}}_n L^{i\epsilon}\right] r^{n-1/2} \Big\{ \omega \big[2\sin\hat{\theta}_1 - \sin\theta_1 + (1-2n)\cos\hat{\theta}_2 \sin\theta - 2\epsilon\sin\hat{\theta}_2 \\ \sin\theta \big] - \sin\hat{\theta}_3/\omega \Big\} + 4\hat{c}_2 \Re[\mathbf{b}_n] r^n \big[\cos n\theta - \cos(n+2)\theta + n\sin\theta \\ \sin(n+1)\theta \big] + 4\hat{c}_2 \Im[\mathbf{b}_n] r^n \big[-\sin n\theta + n\sin\theta\cos(n+1)\theta \big],\end{aligned} \tag{A2}$$

$$\sigma_{r\theta} = \sum_{n=0}^{N} \Re\left[\bar{\mathbf{a}}_n L^{i\epsilon}\right] r^{n-1/2} \Big\{ \omega\left[-\sin\theta_1 + (1-2n)\cos\hat{\theta}_2 \sin\theta - 2\epsilon \sin\hat{\theta}_2 \sin\theta\right] + \sin\hat{\theta}_3/\omega \Big\} + \Im\left[\bar{\mathbf{a}}_n L^{i\epsilon}\right] r^{n-1/2} \Big\{ \omega\left[\cos\theta_1 + (1-2n)\sin\hat{\theta}_2 \sin\theta + 2\epsilon \cos\hat{\theta}_2 \sin\theta\right] + \cos\hat{\theta}_3/\omega \Big\} + 4\hat{c}_2 \Re[\mathbf{b}_n] r^n \left[-n \sin\theta \cos(n+1)\theta - \sin(n+2)\theta\right] + 4\hat{c}_2 \Im[\mathbf{b}_n] r^n \left[n \sin\theta \sin(n+1)\theta\right], \tag{A3}$$

where

$$\theta_1 = (n-1/2)\theta - \phi,$$

$$\theta_2 = (n-3/2)\theta - \phi,$$

$$\theta_3 = (n-1/2)\theta + \phi,$$

$$\hat{\theta}_i = \theta_i + 2\theta,$$

$$\phi = \epsilon \ln(r/2a),$$

$$\omega = \exp(-\epsilon(\pi - \theta)),$$

$$\hat{c}_i = c_i/(c_1 + c_2),$$

$$c_i = (1+\kappa_i)/\mu_i,$$

$L = 2a$, $\kappa_i = 3 - 4\nu_i$ for plane strain and $\kappa_i = (3-\nu_i)/(1+\nu_i)$ for plane stress, and μ_i is the shear modulus. The subscript i takes the value of 1 and 2 corresponding to materials 1 and 2, respectively.

Appendix B. Least-squares analysis

The system of equations for the stress field around the crack tip can be represented in a generic form as

$$\sigma = \sum_{m=0,1,2,\ldots}^{\infty} a_m f_m(r,\theta) \tag{B1}$$

where a_m are the set of coefficients to be determined. The Eq. (B1) can be represented in matrix form as

$$\begin{pmatrix} f_1(r_1,\theta_1) & f_2(r_1,\theta_1) & \dots & f_m(r_1,\theta_1) \\ f_1(r_2,\theta_2) & f_2(r_2,\theta_2) & \dots & f_m(r_2,\theta_2) \\ \vdots & \vdots & \ddots & \vdots \\ f_1(r_n,\theta_n) & f_2(r_n,\theta_n) & \dots & f_m(r_n,\theta_n) \end{pmatrix}_{n\times m} \begin{Bmatrix} a_0 \\ a_1 \\ \vdots \\ a_m \end{Bmatrix}_{m\times 1} = \begin{Bmatrix} \sigma(r_1,\theta_1) \\ \sigma(r_2,\theta_2) \\ \vdots \\ \sigma(r_n,\theta_n) \end{Bmatrix}_{n\times 1} \tag{B2}$$

for n-number data with m terms of the series. The set of data thus obtained can be compactly represented as

$$[A]_{n\times m}\{X\}_m = \{B\}_n. \tag{B3}$$

A solution $\{X\}^*$ of this system of equations is the one that minimizes the squares of residues of $\{V\}_n$ defined by the dot product [21]

$$V^2 = \left([A]\{X\}^* - \{B\}\right)^{\mathrm{T}} \cdot \left([A]\{X\}^* - \{B\}\right), \tag{B4}$$

where the dimensions of the matrices are omitted for clarity. Then, the solution $\{X\}^*$ which minimizes V^2 is the solution of the N equations

$$\frac{\partial V^2}{\partial \{X\}^*} = [A]^{\mathrm{T}}[A]\{X\}^* - [A]^{\mathrm{T}}\{B\}, \tag{B5}$$

or

$$[A]^{\mathrm{T}}[A]\{X\}^* = [A]^{\mathrm{T}}\{B\}, \tag{B6}$$

which can be compactly written as

$$\left[\bar{A}\right]\{X\}^* = \left\{\bar{B}\right\}, \tag{B7}$$

where $[\bar{A}] = [A]^{\mathrm{T}}[A]$ and $\{\bar{B}\} = [A]^{\mathrm{T}}\{B\}$. Care must be taken while inverting the matrix $[\bar{A}]$ which is often ill-conditioned due to the singularities in the problem. Hence, special algorithms such as QR or Household algorithms must be used to ensure stable results.

References

[1] Tippur HV, Ramaswamy S. Measurement of mixed-mode fracture parameters near cracks in homogeneous and bimaterial beams. International Journal of Fracture 1993;61:247–65.

[2] Lu H, Chiang FP. Photoelastic determination of stress intensity factor of an interfacial crack in a bi-material. Journal of Applied Mechanics 1993;60:93–100.

[3] Singh RP, Shukla A. Characterization of isochromatic fringe patterns for a dynamically propagating interface crack. International Journal of Fracture 1996;76:293–310.

[4] Dally JW, Sanford RJ. Strain gage methods for measuring the opening mode stress-intensity factor K_{I}. Experimental Mechanics 1988;27:381–8.

[5] Dally JW, Sanford RJ. Measuring the stress intensity factor for propagating cracks with strain gages. Journal of Testing and Evaluation 1990;18:240–9.

[6] Shukla A, Agarwal BD, Bhushan B. Determination of SIF in orthotropic composite materials using strain gages. Engineering Fracture Mechanics 1989;32:469–77.

[7] Ricci V, Shukla A, Singh RP. Evaluation of fracture parameters in bimaterial system using strain gages. Engineering Fracture Mechanics 1997;58:273–83.
[8] O'Dowd NP, Shih CF, Stout MG. Test geometries for measuring interfacial fracture toughness. International Journal of Solids and Structures 1992;29:571–89.
[9] Dundurs J. In: Mathematical theory of dislocations. New York: ASME, 1969. p. 70–115.
[10] Williams LM. The stress around a fault or crack in dissimilar media. Bulletin of Seismological Society of America 1959;49:199–204.
[11] Hutchinson JW, Mear M, Rice JR. Crack paralleling an interface between dissimilar materials. Journal of Applied Mechanics 1987;54:828–32.
[12] Rice JR. Elastic fracture mechanics concepts for interface crack. Journal of Applied Mechanics 1988;55:98–103.
[13] Sun CT, Jih CJ. On strain energy release rates for interfacial cracks in bi-material media. Engineering Fracture Mechanics 1987;28:13–20.
[14] Shih CF. Cracks on bimaterial interfaces: elasticity and plasticity aspects. Material Science and Engineering 1991;A143:77–90.
[15] Miyazaki N, Ikeda T, Soda T, Munakata T. Stress intensity factor analysis of interface crack using boundary element method — application of contour-integral method. Engineering Fracture Mechanics 1993;45:599–610.
[16] Lee Y, Rosakis AJ. Interface cracks in plates: a 3D numerical investigation. International Journal of Solids and Structures 1993;30:3139–58.
[17] Sinha JK, Tippur HV, Xu L. An interferometric and finite element investigation of interfacial crack-tip fields: role of mode-mixity on 3D stress variations. International Journal of Solids and Structures 1997;34:741–54.
[18] Marur PR, Tippur HV. Evaluation of mechanical properties of functionally graded materials. Journal of Testing and Evaluation 1998;26:539–45.
[19] Sanford RJ. Determining fracture parameters with full-field optical methods. Experimental Mechanics 1989;29:241–7.
[20] Marur PR. Numerical simulation of anvil interaction in the impact testing of notched bend specimens. International Journal of Fracture 1996;81:27–37.
[21] L.E. Hulbert, The numerical solution of two-dimensional problems of the theory of elasticity, Ohio State University, Columbus, OH.